Plume Characterization of Gas-Fed Pulsed Plasma Deflagration Thrusters

IEPC-2015-434p／ISTS-2015-b-434p

Presented at Joint Conference of 30th International Symposium on Space Technology and Science, 34th International Electric Propulsion Conference and 6th Nano-satellite Symposium
Hyogo-Kobe, Japan
July 4–10, 2015

Keith T. K. Loebner*, Thomas C. Underwood†, Andrea Lucca Fabris‡, and Mark A. Cappelli§
Stanford University, Stanford, CA, 94305, U.S.A.

and

James J. Szabo¶
Busek Co. Inc., Natick, MA, 01760, U.S.A.

We present experimental studies of two prototype gas-fed pulsed plasma thrusters designed to operate in the well-known deflagration mode. Several thruster configurations were examined, including multiple electrode geometries, current-drive polarities, and gas-injection methods. A quadruple Langmuir probe operating in current-saturation mode was used to obtain time-resolved measurements of the plasma density, temperature, potential, and velocity throughout the thruster plume. A fast-framing, intensified CCD camera was used to image the evolution of the plume over a single pulse for each thruster configuration. We identify the transition between operating modes that occurs as the result of various tested thruster configurations, and prescribe a path towards a practical gas-fed pulsed plasma deflagration thruster based on our observations.

Nomenclature

A	= probe area
d_s	= probe sheath thickness
e	= elementary charge
I	= current
$J_{e0,i0}$	= electron/ion current density
k	= Boltzmann constant
m_i	= ion mass
n	= species number density
r_p	= probe radius
S_i	= ion Mach number
T	= temperature
Z_i	= ion charge number
ϕ	= electric potential
λ_D	= Debye radius

*Ph.D. Candidate, Mechanical Engineering Department, kloebner@stanford.edu
†Graduate Student, Mechanical Engineering Department, tunderw5@stanford.edu
‡Postdoctoral Researcher, Mechanical Engineering Department, lfandrea@stanford.edu
§Professor, Mechanical Engineering Department, cap@stanford.edu
¶Chief Scientist for Hall Thrusters, Busek Co., jszabo@busek.com

I. Introduction

PULSED plasma thrusters are an important class of electric propulsion devices, providing a number of advantages over other ion accelerators.

The deflagration mode in gas-fed pulsed plasma accelerators was first identified and studied by Cheng,[1] who also considered its application to space propulsion. It has several advantages over the more frequently seen 'detonation' or 'snow-plow' mode, such as increased electrostatic to kinetic energy conversion efficiency and reduced electrode erosion. The governing physics of the plasma deflagration has been investigated further by others,[2–9] but a practical implementation as a small-to-medium-sized electric propulsion system has not yet been realized. In this work, we investigate a thruster designed specifically with low average power and high specific impulse in mind, as these attributes are required for such a system.

Utilizing a quadruple Langmuir probe in current-saturation mode, we make time-resolved measurements of the plasma properties in the plume of two different thrusters. We also use a fast-framing ICCD camera to make qualitative observations of the discharge characteristics at multiple times during a single firing of the thruster. We compare and contrast the behavior of the thrusters operated under various conditions, and indicate the apparent optimal operating mode in order to achieve maximal directed plume kinetic energy.

II. Experimental Facility & Apparatus

A. Vacuum Chamber

All experiments were carried out in a subsection attached to the Large Vacuum Chamber (LVC) at Stanford University. The subsection, shown in Fig. 3, consists of a 6" internal diameter Pyrex tube with Conflat flanges at either end, coupled to a 6" Conflat T-section, which is in turn mated to a six-way cross before finally linking to the LVC (schematic shown in Fig. 1). The subsection is separated from the LVC by a pneumatic gate valve. All tests reported here were performed at a nominal background pressure of 10^{-7} Torr, backed by two cryopumps.

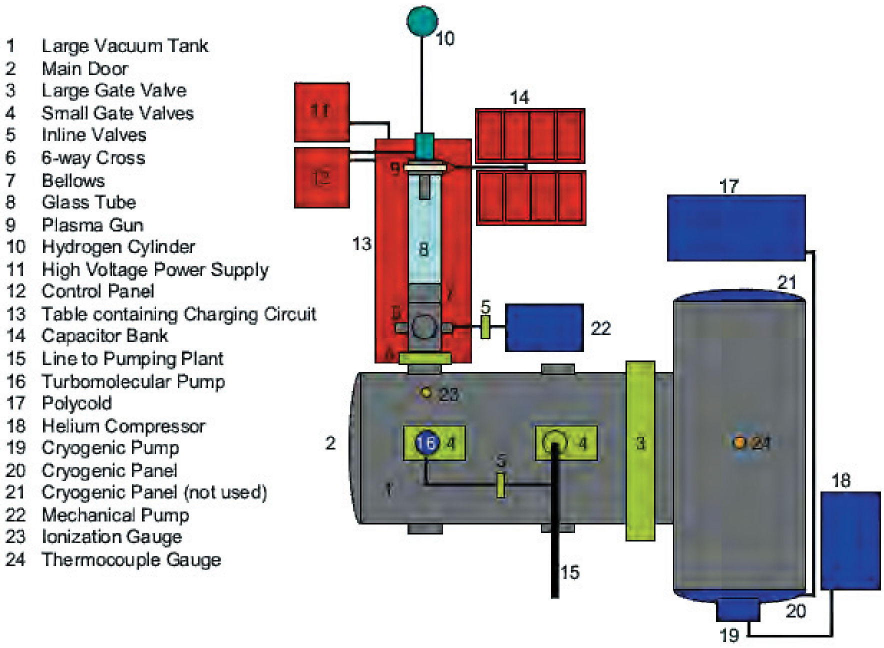

Figure 1: Labeled schematic layout of the Large Vacuum Chamber and the gun section, along with the energy banks.

B. Power System

The power system is shown in Fig. 1. The energy storage consists of a bank of one to four oil-filled, 14 μF capacitors. The number of capacitors in the bank can be varied manually. A low-inductance (15 nH) transmission line connects the capacitor to the thruster electrodes outside the vacuum chamber. The capacitor is charged to the specified discharge voltage by a TDK-Lambda 500A capacitor-charging power supply, which is isolated from the thruster circuit prior to firing. When the thruster is fired, the resulting current waveform (an example of which is shown in Fig. 4b) is an approximately free-ringing damped LCR oscillation, with a characteristic period of $\sim$20 μs.

C. Thrusters

Two thrusters were used in these experiments, driven by the same power system. The first thruster is an integrated unit designed as a stand-alone thruster, containing a microfluidic pulsed solenoid valve as a gas injector and a solid coaxial electrode configuration. The second thruster is of a modular design, enabling modification of the electrode geometry. This second thruster is based on a larger device employed in high-energy plasma acceleration, the Stanford Plasma Gun. It contains a custom-built puff valve specifically constructed to provide a sharp density front at the breech of the coaxial electrode arrangement, which has been shown to be a necessary condition for a deflagration mode to occur.[10]

Both thrusters were sealed to 6" Conflat flanges so that they could be mounted directly to the vacuum chamber, and each thruster was made to pass through its corresponding flange such that the electrodes were accessible from outside the vacuum.

(a) Photograph of the SBT, not mounted to the CF flange.

(b) Photograph of the M-SPG thruster, mounted to the CF flange.

Figure 2

1. *Stanford-Busek Thruster*

The Stanford-Busek Thruster is shown in Fig. 2a. The electrode assembly consists of a solid outer cylindrical conductor made of stainless steel, with a copper center electrode. The outer electrode is 5 cm in outer diameter, while the outer diameter of the center electrode is 0.75 cm. The copper center electrode fastens to a copper backplate, through which the injected gas flows via a set of gas-distribution inlets (shown in Fig. 2a). The electrodes are held at high potential, separated by a sealed insulator, and breakdown is initiated by the gas puff entering the interelectrode region.

2. *Miniature Stanford Plasma Gun*

The Miniature Stanford Plasma Gun (M-SPG) is designed to mimic the bulk geometry of the SBT, but includes an advanced custom-built puff valve to increase the density of the injected gas as well as a rod-electrode configuration for the outer electrode. The rod anode configuration (shown in Fig. 2b) both alters the inductance per unit length of the thruster, and also allows residual gas and unaccelerated neutrals to diffuse radially away from the center electrode after the plasma is ignited.

III. Experimental Methods & Diagnostics

A. Quadruple Langmuir Probe

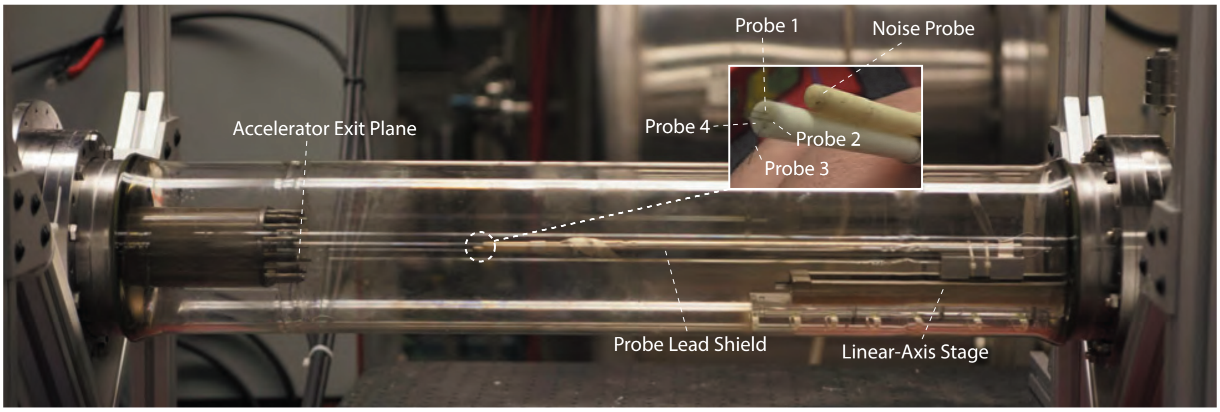

Figure 3: Image of the glass gun section, with the quadruple Langmuir probe (QLP) and linear axis stage installed. The accelerator to the left of the image is the large Stanford Plasma Gun, the valve and flange of which are the basis for the Miniature Stanford Plasma Gun (M-SPG)

A quadruple Langmuir probe (QLP) was used to obtain simultaneous time-resolved measurements of the plasma density, temperature, potential, and ion Mach number at a single spatial point along the acceleration axis of the thruster plume. The QLP was mounted to a linear axis stage, and moving the probe along the axis over the course of multiple firings enabled the compilation of a spatiotemporal contour of each of the plasma state variables.

Quadruple Langmuir probes are an immersed diagnostic that allow simultaneous monitoring of four plasma state variables. For this study, a QLP was constructed and operated in current-saturation mode to obtain time-resolved measurements of the resulting plasma plume.[11] The probe as constructed consists of four independent electrodes, as shown in Fig. 4a. Electrodes 1,2, and 4 are oriented parallel to the flow direction while electrode 3 is perpendicular to the flow direction. Electrodes 3 and 4 are nominally biased at -18 V with respect with electrode 1 (ϕ_{13} and ϕ_{14}) while electrode 2 is biased at -3 V (ϕ_{12}).

In order to calculate the plasma state variables of interest, the measured current and associated bias voltages must be coupled together with current collection theory. Similar to other electrostatic probes, the current collected by the probe, I_p, is composed of contributions due to both electrons and ions and can be given as,

$$I_p = I_e - I_i, \tag{1}$$

where I_e and I_i correspond to collected current due to electrons and ions respectively. For any of the probes exposed to the plasma flow, electron current will be collected if the probe potential is less than the plasma potential ($\phi_{\text{probe}} \leq \phi_{\text{plasma}}$) according to,

$$I_{\|e} = A_{\text{probe}} J_{e0} \exp\left[-\frac{e}{kT}\left(\phi_{\text{plasma}} - \phi_{\text{probe}}\right)\right], \tag{2}$$

which is a function of both the parallel or perpendicular probe area exposed to plasma, A_{probe}, and the thermal diffusion of electrons. Ion current collection however is a more complicated function of the operational regime of the probe and more specifically the local probe radius to Debye length ratio, r_p/λ_D, and ion to electron temperature ratio, T_i/Z_iT_e. If $5 \leq r_p/\lambda_D \leq 100$ and T_e/Z_iT_i, Ref. 12 developed a relationship for ion current collection as a function of empirical fitting parameters α and β via an algebraic fit to experimental

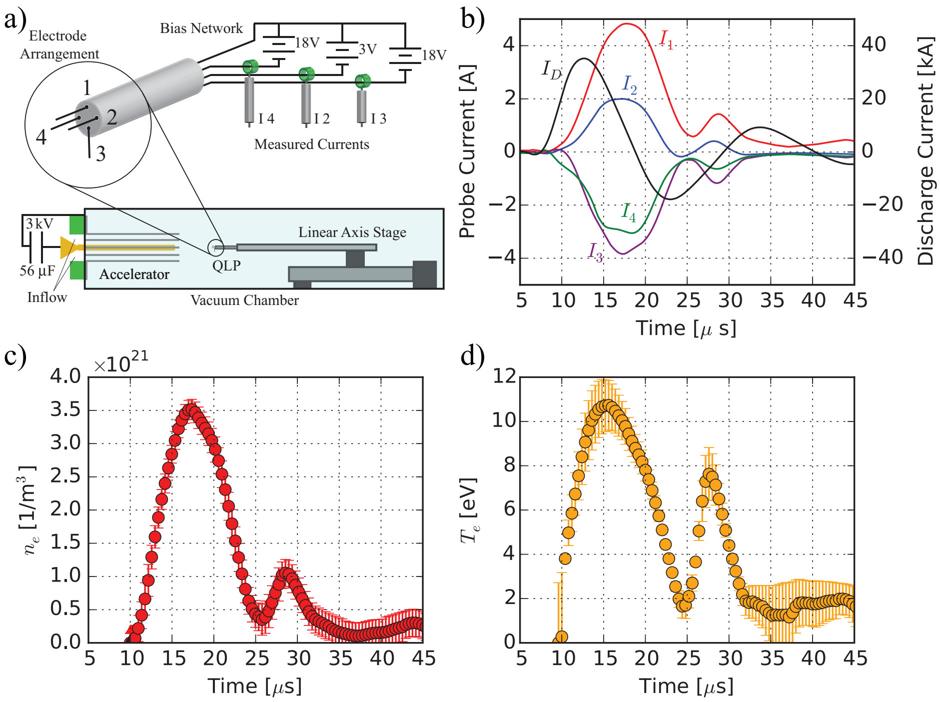

Figure 4: Schematic illustrating the use of the QLP. **(a)** A schematic of the probe and the bias network. **(b)** Example probe and discharge current traces. **(c)** A plot of the calculated plasma density as a function of time. **(d)** A plot of the calculated plasma temperature as a function of time.

measurements,[13]

$$I_{\parallel i} = A_{\mathrm{probe}} J_{i0} \left(\beta + \frac{e}{kT} \left(\phi_{\mathrm{plasma}} - \phi_{\mathrm{probe}} \right) \right)^{\alpha}, \tag{3}$$

$$\alpha = \frac{2.9}{\ln(r_p/\lambda_D) + 2.3} + 0.07 \left(\frac{T_i}{Z_i T_e} \right)^{0.75} - 0.34, \tag{4}$$

$$\beta = 1.5 + \frac{T_i}{Z_i T_e} \left[0.85 + 0.135 \left(\ln \left[\frac{r_p}{\lambda_D} \right] \right)^3 \right]. \tag{5}$$

An analytical expression for the ion current collected by the perpendicular probe was obtained by assuming a negligible sheath thickness[14] $d_s/r_p \to 1$,

$$I_{\perp i} = A_{\perp} n_e e \left(\frac{kT}{2\pi m_e} \right)^{1/2} \frac{2}{\sqrt{\pi}} \exp\left[-S_i^2 \right] \sum_{j=0}^{\infty} \frac{S_i^j}{j!} \Gamma \left(j + \frac{3}{2} \right). \tag{6}$$

By combining these relationships for each probe and assuming quasineutrality ($n_e = n$) and thermal equilibrium ($T_i = T_e$) within the plasma, a set of four coupled nonlinear equations can be developed and solved for each of the plasma state variables at each point in time,

$$I_1 = A_{\parallel} J_{e0} \exp\left(-\frac{e\phi_{p1}}{kT}\right) - A_{\parallel} J_{i0}\left(\beta + \frac{e\phi_{p1}}{kT}\right)^{\alpha}, \tag{7}$$

$$I_2 = A_{\parallel} J_{e0} \exp\left(-\frac{e(\phi_{p1}+\phi_{12})}{kT}\right) - A_{\parallel} J_{i0}\left(\beta + \frac{e(\phi_{p1}+\phi_{12})}{kT}\right)^{\alpha}, \tag{8}$$

$$I_3 = A_{\parallel} J_{e0} \exp\left(-\frac{e(\phi_{p1}+\phi_{13})}{kT}\right) - A_{\parallel} J_{i0}\left(\beta + \frac{e(\phi_{p1}+\phi_{13})}{kT}\right)^{\alpha}, \tag{9}$$

$$I_4 = A_{\perp} J_{e0} \exp\left(-\frac{e(\phi_{p1}+\phi_{14})}{kT}\right) - A_{\perp} n_e e \left(\frac{kT}{2\pi m_e}\right)^{1/2} \frac{2}{\sqrt{\pi}} \exp\left(-S_i^2\right) \sum_{j=0}^{\infty} \frac{S_i^j}{j!}\Gamma\left(j+\frac{3}{2}\right). \tag{10}$$

In the event that $r_p/\lambda_D > 100$, the ion collection theory used in Eqn. 3 is invalid. In this case, a thin sheath is assumed and the ion current follows a Bohm expression,[15]

$$I_{\parallel i} = A_{\parallel} n_e e \sqrt{\frac{kT}{m_i}} \exp\left(-\frac{1}{2}\right) \tag{11}$$

Replacing the associated ion collection contributions for probes 1-3 yields the system of equations valid for a thin sheath $r_p/\lambda_D > 100$,

$$I_1 = A_{\parallel} J_{e0} \exp\left(-\frac{e\phi_{p1}}{kT}\right) - A_{\parallel} n_e e \sqrt{\frac{kT}{m_i}} \exp\left(-\frac{1}{2}\right) \tag{12}$$

$$I_2 = A_{\parallel} J_{e0} \exp\left(-\frac{e(\phi_{p1}+\phi_{12})}{kT}\right) - A_{\parallel} n_e e \sqrt{\frac{kT}{m_i}} \exp\left(-\frac{1}{2}\right) \tag{13}$$

$$I_3 = A_{\parallel} J_{e0} \exp\left(-\frac{e(\phi_{p1}+\phi_{13})}{kT}\right) - A_{\parallel} n_e e \sqrt{\frac{kT}{m_i}} \exp\left(-\frac{1}{2}\right) \tag{14}$$

$$I_4 = A_{\perp} J_{e0} \exp\left(-\frac{e(\phi_{p1}+\phi_{14})}{kT}\right) - A_{\perp} n_e e \left(\frac{kT}{2\pi m_e}\right)^{1/2} \frac{2}{\sqrt{\pi}} \exp\left(-S_i^2\right) \sum_{j=0}^{\infty} \frac{S_i^j}{j!}\Gamma\left(j+\frac{3}{2}\right) \tag{15}$$

Each of the nonlinear systems described by Eqns. 7-10 and Eqns. 12-15 are solved using a Newton-Raphson algorithm with a centered trust region. Initial estimates of each state variable are obtained by algebraic reduction of each system. In order to ensure application of the correct ion collection model, the system of equations derived assuming a thin sheath are initially solved and the resulting Debye length is computed. If r_p/λ_D is such that the theory developed in Ref.[13] is valid, the state variables are recalculated.

B. Fast-Framing Imaging

In order to characterize the general behavior of each thruster configuration, a Cordin 220-UV ICCD camera was used to obtain several frames of the optical emission produced by the plasma during each discharge event. The operation mode of the thruster, i.e. detonation/snow plow or deflagration, was determined based in part on the observed evolution of the accelerated plasma.

IV. Variational Studies: Results & Discussion

A. Drive-Current Polarity

The first set of experiments was performed on the SBT device, operated at a constant energy of 44 J per pulse on a single capacitor (corresponding to a charging voltage of 2.5 kV). A full QLP contour was collected for each polarity condition. In the first case, the contour of which is shown in Fig. 5a, the center electrode of the SBT was positively charged and the conventional current direction (ion current) was driven radially outward. The contour in Fig. 5b shows the second case, in which the center electrode of the SBT was negatively charged and the ion current was driven radially inwards. The white regions in both figures are noise due to the fact that the QLP system of equations does not solve here, since the first real signal due to plasma contact with the probe is represented by the lower edge of the contour. The difference in the time

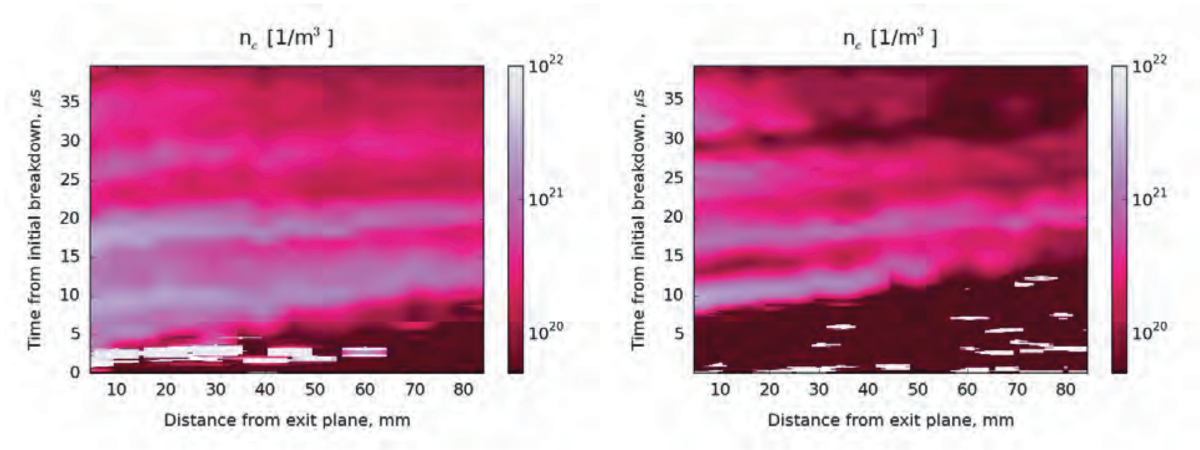

(a) Plasma density contour of the SBT operated in outer-cathode, 'positive-polarity' mode.

(b) Plasma density contour of the SBT operated in inner-cathode, 'negative-polarity' mode.

Figure 5

from initial breakdown between the two test cases is due to different trigger levels on the oscilloscope, which was triggered by the discharge current.

From a purely magnetohydrodynamic perspective, the direction of the current should not alter the acceleration process; the vector of the Lorentz force remains in the axial direction. However, it is clear from the results that the behavior of the thruster is substantially different between each case. The multiple expelled plasma plumes are visible as striations in the contours, and the velocity of the plume can be estimated from the slope of the leading edge of the contour. In the positive-polarity case, there is not a significant drop in plasma density along the axis between the first two acceleration events. Contrasted with the negative-polarity mode, where a clear separation is seen in time between the first two events, this indicates that the plumes are localized more strongly in time when the center electrode is the cathode. One explanation of this phenomenon is that the ions are accelerated radially inwards as well as axially in the negative-polarity case, leading to a collimated jet on the axis and an overall less-diffuse accelerated plasma plume.

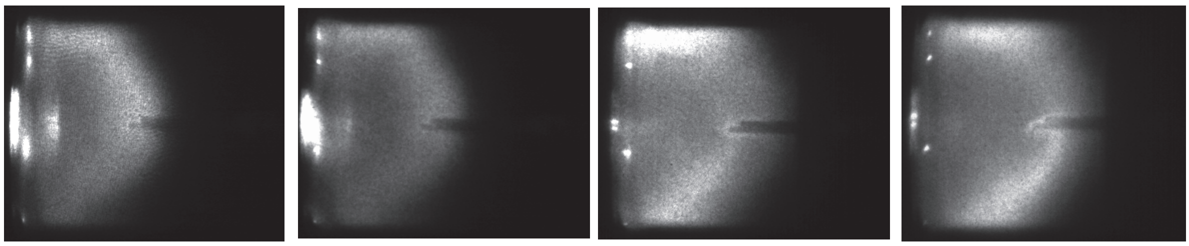

(a) 5 μs (b) 6 μs (c) 7 μs (d) 8 μs

Figure 6: Fast framing images of a representative firing of the SBT in positive-polarity mode.

The ICCD images, shown in Figs. 6 and 7, show clearly that in the positive-polarity case, the thruster is operating in a detonation or snow-plow mode. This is indicated by what appears from the images to be a plasma sheet propagating axially away from the thruster exit. The thruster exit is not visible in the images in either case. In the negative-polarity case, for the same ICCD gain settings and frame timing, we observe a radically different behavior even at the same charging energy. Instead of a propagating sheet, there is a much brighter region concentrated nearer to the central axis. There may be a less-strongly emitting plasma that is further downstream than this region but is invisible on the CCD array due to its significantly lower emission strength.

The most probable explanation for this behavior is that the ion current is driven radially inwards in the negative-polarity case, such that the strongly-emitting excited ion species are concentrated about the center

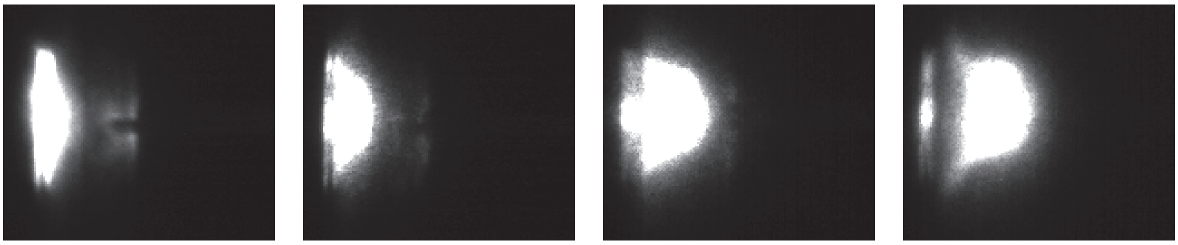

(a) 5 μs (b) 6 μs (c) 7 μs (d) 8 μs

Figure 7: Fast framing images of a representative firing of the SBT in negative-polarity mode.

electrode. Though we do calculate a higher plume velocity in the negative-polarity case (∼12 km/s vs ∼10 km/s), the difference is within the error of our method of calculating the overall plume velocity on the basis of the contour composed of an ensemble of shots. From a propulsion perspective, however, it is clear that the overall directed kinetic energy is higher in the negative-polarity case based on the observations of the plume itself. The reduction of the diffuse character of the accelerating plume in the tube section is an indication that in the space environment, plume divergence would be significantly less for a thruster employing the polarity shown in Fig. 7.

B. Geometry & Gas-Injection

In order to compare the effects of electrode geometry and gas injection methods on the plume characteristics, the M-SPG thruster was employed (shown in Fig. 2b). The rod-anode configuration allows the gas to expand radially as well as axially while inside the electrode volume, which should decrease the upstream residual gas density during repeated pulses. The gas-injection method in this thruster is a custom-built puff valve designed expressly for the introduction of high density gas puffs into the inter-electrode region. It has been observed by several researchers that high density gas puffs, as well as low upstream density, are integral to accessing the deflagration mode.

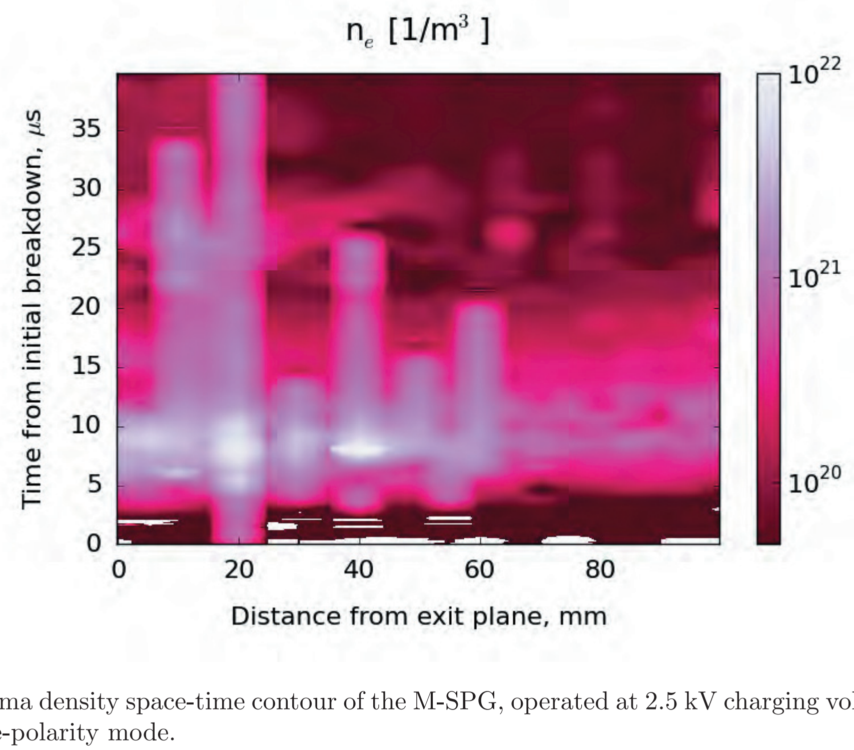

Figure 8: Plasma density space-time contour of the M-SPG, operated at 2.5 kV charging voltage (44 J/pulse) in the negative-polarity mode.

The QLP contour of the plasma density for the M-SPG thruster is shown in Fig. 8. The thruster was operated in the negative-polarity mode, at the same energy of 44 J/pulse. The probe behavior during this test was somewhat erratic, as evidenced by the streaks of high calculated plasma density in the contour; these are not physically meaningful, and are the result of probe currents that did not return to zero in the observed time window and thus the equations did not converge to a reasonable value. However, the leading edge of the plume is still visible and a plume time-of-flight velocity can be calculated. For the M-SPG, we calculate a velocity of ∼37 km/s, which is approximately a factor of four higher than both the negative and positive-polarity operating modes of the SBT.

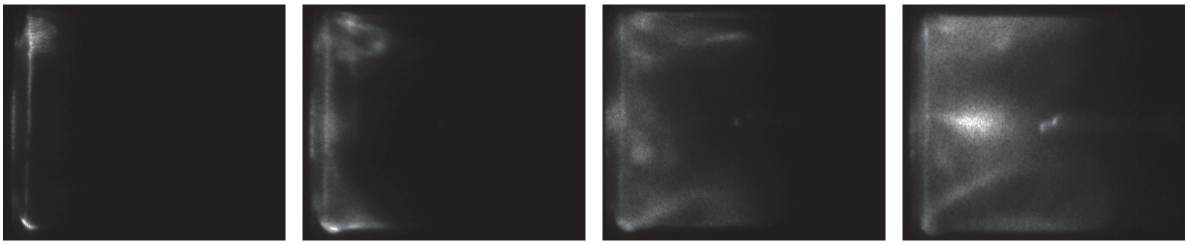

(a) 5 μs (b) 6 μs (c) 7 μs (d) 8 μs

Figure 9: Fast framing images of a representative firing of the M-SPG in negative-polarity mode.

A series of ICCD images of the M-SPG in operation are shown in Fig. 9. As we can see in the photographs, the rod-anode configuration allows a substantial amount of the processes gas to escape around the periphery. However, there is a localized jet that emerges from the gun as well. Based on the QLP data, this axial jet has a significantly higher velocity than the on-axis plume produced by both sets of SBT experiments.

V. Conclusion

In this work, we have presented data and observations concerning the operation of two gas-fed pulsed plasma thrusters designed for operation in a plasma deflagration regime. Through careful experiments we have measured the plume velocity of the SBT system in both a positive-polarity and negative-polarity mode, and found the plume parameters and velocity along the axis to be similar but with vastly different observable characteristics. The expelled plasma of the former mode behaves as a radially-expanding, quasi-spherical sheet followed by a diffuse plasma that fills the test section. The latter mode, by contrast, behaves as a substantially more collimated, brighter plasma plume that expands axially downstream, indicating that the thrust efficiency in the negative-polarity mode should be greater.

The M-SPG thruster was used to test whether ‘sharpness’ of the injected gas puff plays a role in the observed plume conditions, as it employs a specialized valve designed to inject such a gas puff instead of the commercial microfluidic valve incorporated into the SBT. We found that significantly higher axial velocities were observed using the M-SPG thruster, while keeping all other operating condition variable the same. In future work, we will replace the rod-anode configuration with an enclosed outer electrode as in the SBT design, in order to de-couple the impact of the custom valve and anode design on the plume characteristics.

Based on these preliminary results, we see great potential in a gas-fed pulsed plasma deflagration thruster employing a high-density gas puff valve. The high plume velocity, if it can be extended to the remainder of the injected gas by containing it within the electrode volume to be ionized and accelerated, would enable a high I_{sp} and low average power pulsed electric propulsion system, capable of providing orbit-transfer or station-keeping capacity to a host of small and medium-size spacecraft.

Acknowledgments

The authors would like to thank all members of the Stanford Plasma Physics Laboratory for their helpful discussions and guidance. The development of the SBT was supported by the Air Force Office of Scientific Research (AFOSR), with Mitat Birkan as program manager. The construction and testing of the quadruple Langmuir probe was supported by the U.S. Department of Energy, Grant No. DE-NA0002011. K. Loebner and T. Underwood acknowledge Government support under and awarded by DoD, Air Force

Office of Scientific Research, National Defense Science and Engineering Graduate (NDSEG) Fellowship, 32 CFR 168a.

References

[1]Cheng, D. Y., "Plasma deflagration and the properties of a coaxial plasma deflagration gun," *Nuclear Fusion*, Vol. 10, No. 3, Sept. 1970, pp. 305–317.

[2]Baum, P. and Bratenahl, A., "the laboratory magnetosphere," *Geophysical Research Letters*, Vol. 9, No. 4, 1982, pp. 435–438.

[3]Woodall, D. M. and Len, L. K., "Observation of current sheath transition from snowplow to deflagration," *Journal of Applied Physics*, Vol. 57, No. 3, 1985, pp. 961.

[4]Degnan, J. H., Baker, W. L., Warren, S. W. R., Price, D. W., Snell, M. P., Richter-Sand, R. J., and Turchi, P. J., "Puff-gas coaxial-injected electromagnetic coaxial plasma gun," *Journal of Applied Physics*, Vol. 61, No. 8, 1987, pp. 2763.

[5]Wallace, R., *Theoretical, computational and experimental analysis of the deflagration plasma accelerator and plasma beam characteristics*, Ph.D. thesis, Virginia Polytechnic Institute and State University, 1991.

[6]Dahlen, G., Baum, P., and Cheng, D., "PLASMA THRUSTERS FOR LOW FLYING SATELLITES: A SPACE TELEPHONE SYSTEM APPLICATION," *Proceedings of the 23rd . . .*, 1993, pp. 192–199.

[7]Bradley, J. T., "Pulsed power diagnostics on the pladis," 1995, pp. 897–902.

[8]Poehlmann, F. R., Cappelli, M. A., and Rieker, G. B., "Current distribution measurements inside an electromagnetic plasma gun operated in a gas-puff mode." *Physics of plasmas*, Vol. 17, No. 12, Dec. 2010, pp. 123508.

[9]Loebner, K. T. K., Wang, B. C., Poehlmann, F. R., Watanabe, Y., and Cappelli, M. A., "High-Velocity Neutral Plasma Jet Formed by Dense Plasma Deflagration," *IEEE Transactions on Plasma Science*, Vol. 42, No. 10, Oct. 2014, pp. 2500–2501.

[10]Loebner, Keith T. K., Underwood, Thomas C., Cappelli, M. A., "A fast rise-rate, adjustable-mass-bit gas puff valve for energetic pulsed plasma experiments," .

[11]Gatsonis, N. A., Zwahlen, J., Wheelock, A., Pencil, E. J., and Kamhawi, H., "Characterization of a pulsed plasma thruster plume using a quadruple langmuir probe method," *AIAA Paper*, Vol. 4123, 2002, pp. 2002.

[12]Peterson, E. and Talbot, L., "Collisionless electrostatic single-probe and double-probe measurements," *AIAA Journal*, Vol. 8, No. 12, 1970, pp. 2215–2219.

[13]Laframboise, J., "Theory of cylindrical and spherical Langmuir probes in a collisionless plasma at rest," *Rarefied Gas Dynamics, Volume 2*, Vol. 1, 1965, p. 22.

[14]Johnson, B. H. and Murphree, D., "Plasma velocity determination by electrostatic probes," *AIAA Journal*, Vol. 7, No. 10, 1969, pp. 2028–2030.

[15]Chen, S.-L. and Sekiguchi, T., "Instantaneous direct-display system of plasma parameters by means of triple probe," *Journal of Applied Physics*, Vol. 36, No. 8, 1965, pp. 2363–2375.